

Chemical kinetic modeling of organic pollutant degradation in Fenton and solar photo-Fenton processes

Yu Li, Hefa Cheng*

MOE Laboratory for Earth Surface Processes, College of Urban and Environmental Sciences, Peking University, Beijing 100871, China

ARTICLE INFO

Article History:

Received 24 February 2021

Revised 27 April 2021

Accepted 9 May 2021

Available online 24 May 2021

Keywords:

Fast kinetics

On-line spectrophotometric detection

Chemical kinetic model

Hydroxyl radical

Organic pollutant treatment

ABSTRACT

The oxidation of organic pollutants by Fenton's reagent is commonly considered as a single-stage process that conforms to pseudo first-order kinetics. However, pollutant oxidation would exhibit a two-stage pattern when the initial dosage of Fenton's reagent is sufficiently high. This study investigated the fast oxidation kinetics of a model pollutant, malachite green (MG), in Fenton process in real time using continuous on-line spectrophotometric detection. A chemical kinetic model was further developed, which could well predict the effect of initial concentrations of Fe^{2+} , H_2O_2 , and MG on the degradation of MG in Fenton and solar photo-Fenton processes. The model could also be adapted to model the kinetics of MG mineralization. Modeling results reveal that the significant enhancement in the degradation rate of MG in the second stage of Fenton process by sunlight irradiation was contributed mainly by the production of hydroxyl radicals from H_2O_2 photolysis. The chemical kinetic model also performed well in describing the degradation and mineralization kinetics of carbendazim and thiabendazole in solar photo-Fenton process. The improved understanding on the fast kinetics of pollutant degradation and the chemical kinetic model developed could help optimize the treatment conditions for organic pollutants in Fenton and solar photo-Fenton processes.

© 2021 Taiwan Institute of Chemical Engineers. Published by Elsevier B.V. All rights reserved.

1. Introduction

Advanced oxidation processes (AOPs) hold promises for the treatment of a wide range of refractory organic pollutants [1–3]. Fenton process is a common type of AOPs that has been employed extensively in wastewater treatment [4], which could degrade most organic compounds due to the generation of hydroxyl radicals ($\cdot\text{OH}$) [5]. The concentration of $\cdot\text{OH}$ is often considered to be steady throughout the treatment process, thus the degradation kinetics of organic pollutants in Fenton process is commonly described by the first-order kinetic model [6,7]. Nonetheless, deviation in the pollutant degradation kinetics from first-order has been observed [8].

A two-stage decomposition phenomenon would occur when the dosage of Fenton's reagent is sufficiently high [9]. The first stage is dominated by the reaction between Fe^{2+} and H_2O_2 , which occurs rapidly. The production rate of $\cdot\text{OH}$ declines quickly in this stage, thus a steady-state concentration of $\cdot\text{OH}$ could not be maintained, and pollutant degradation would no longer observe pseudo first-order kinetics. The second stage is dominated by the reaction between Fe^{3+} and H_2O_2 . The continuous reduction of Fe^{3+} promotes Fe^{2+} regeneration, resulting in a rather low, but steady concentration of Fe^{2+} [10]. The rate of pollutant oxidation in the second stage is much slower. Experimentally, due to the very fast pollutant degradation in the first stage,

the degradation kinetics could not be well observed or studied using conventional time-sampling techniques.

Photo-Fenton process is a type of modified Fenton treatment that employs UV–visible light irradiation to enhance the oxidation and mineralization of organic pollutants in Fenton process [11,12]. The enhancement effect of light was commonly attributed to Fe^{2+} regeneration from Fe^{3+} photo-reduction ($\text{Fe}^{3+} + \text{H}_2\text{O} + h\nu \rightarrow \text{Fe}^{2+} + \text{OH} + \text{H}^+$, $\lambda < 450 \text{ nm}$) [13], while the extra production of $\cdot\text{OH}$ through H_2O_2 photolysis ($\text{H}_2\text{O}_2 + h\nu \rightarrow 2 \cdot\text{OH}$, $\lambda < 400 \text{ nm}$) was often neglected [14,15]. Nonetheless, the specific contribution of Fe^{3+} photo-reduction and H_2O_2 photolysis to $\cdot\text{OH}$ production in photo-Fenton process has not been quantitatively evaluated.

Several chemical kinetic models have been developed for describing the degradation of organic pollutants in Fenton-type processes. They could predict the changes in the concentrations of chemical species participating in the reactions [16,17], and thus facilitate the design and optimization of treatment conditions [18]. However, none of the chemical kinetic models developed so far could simulate the fast kinetics of pollutant degradation occurring in the first stage of Fenton process, probably due to the challenges in acquiring fast kinetic data [18,19]. Chan and Chu observed two-stage kinetics in the degradation of atrazine and 2,4-dichlorophenoxyacetic acid in Fenton process [20,21], and developed an empirical kinetic model for such behavior, which was named as the BMG model later by Behnajady and co-workers [22]. The BMG model was further applied successfully to describe the reaction kinetics of a range of organic pollutants

* Corresponding author.

E-mail address: hefac@umich.edu (H. Cheng).

in Fenton process, such as the discoloration of dyes [23–25], and the degradation of dimethyl sulfoxide and *N,N*-dimethylacetamide [26]. Tunc and co-workers studied the discoloration of dyes in Fenton process with an online spectrophotometric method [27,28]. Based on comparison of the performance of different kinetic models in describing the reaction kinetics, they found that the BMG model gave the best results [27,28]. Despite its good performance, the BMG model is completely empirical, and the predictions are not based on the suite of chemical reactions occurring in Fenton process.

Understanding the fast kinetics of pollutant degradation in the first stage and its modeling are important for designing efficient Fenton treatment with short reaction times. To obtain pollutant degradation data with high temporal resolution, we chose malachite green (MG) as a model organic pollutant, and used a spectrophotometer with flow cell connected to the reactor for on-line monitoring during the course of Fenton and solar photo-Fenton processes. A detailed chemical kinetic model was developed to describe the degradation kinetics of MG, particularly the fast kinetics in the first stage. The performance of the model was validated under a wide range of conditions, then it was further applied to evaluate the degradation of MG in solar photo-Fenton process. The performance of the chemical kinetic model was further validated with predicting the degradation of two benzimidazole fungicides widely used in agriculture, carben-dazim (CBZ) and thiabendazole (TBZ), in solar photo-Fenton process. To the best of our knowledge, this study is the very first attempt to examine and model the fast kinetics of pollutant degradation in Fenton and solar photo-Fenton processes under high dosages of Fenton's reagent.

2. Materials and methods

2.1. Chemicals and reagents

Malachite green (MG) and $\text{FeSO}_4 \cdot 7\text{H}_2\text{O}$ were purchased from Sino-pharm Chemical Reagent (Beijing, China). H_2O_2 (30 wt.%) was provided by Beijing Institute of Chemical Reagents (Beijing, China), and the content of H_2O_2 was determined by KMnO_4 titration prior to use [29]. 1,10-Phenanthroline (97%) was supplied by Sahn Chemical Technology (Shanghai, China). Tert-butyl alcohol (TBA) was obtained from Xilong Chemical (Guangzhou, China). Acetophenone (AP) was purchased from Xianding Biotechnology (Shanghai, China). CBZ (98%) and TBZ (98%) were purchased from Macklin Biochemical (Shanghai, China). All chemicals were used as received. All solutions were prepared with ultrapure water produced from a Milli-Q water purification system (Millipore, Bedford, MA).

2.2. Fenton and solar photo-Fenton treatment

To monitor MG degradation in real time in Fenton and solar photo-Fenton processes, a continuous on-line spectrophotometric detection system was developed (Fig. S1). The solution temperature was maintained at 25 °C by a re-circulating thermostat bath. The light absorbance of the solution within the flow cell, which was connected to the reactor, was measured continuously at a frequency of 10 Hz. With fast circulation of solution, the chemical composition of solution in the flow cell could be deemed essentially the same as that in the reactor. A UV-3200 UV-visible spectrophotometer (Mapada, Shanghai, China) was used to detect the concentration of MG at 617 nm, with the data collected by the UV-Vis Analyst software supplied by the instrument manufacturer.

In solar photo-Fenton process, a CEL-S500E7 solar simulator equipped with a 500 W short arc xenon lamp and an AM1.5 filter (Ceaulight Technology, Beijing, China) was employed as the light source. Both the emitted wavelength spectrum (between 360 and 1100 nm) and the total irradiance ($96.8 \text{ mW} \cdot \text{cm}^{-2}$) of the solar simulator are close to those of natural sunlight (Fig. S2a). MG degradation

in the presence of Fenton's reagent under the simulated sunlight irradiation was monitored. CBZ and TBZ degradation in solar photo-Fenton process was also conducted, with their degradation tracked using the conventional time-sampling method.

2.3. Analytical methods

The concentration of Fe^{2+} during the course of reaction was determined by the 1,10-phenanthroline colorimetric method [30]. AP was measured on an LC-20A high performance liquid chromatograph (HPLC) equipped with an SPD-M20A photo-diode array detector (Shimadzu, Kyoto, Japan) at the wavelength of 245 nm. The analyte was separated on a WondaSil C18 column ($4.6 \times 50 \text{ mm}$, $5 \mu\text{m}$) using isocratic elution with water and methanol (60:40, v/v) at a flow rate of $0.4 \text{ mL} \cdot \text{min}^{-1}$. CBZ and TBZ were analyzed by HPLC at the wavelength of 220 and 300 nm, respectively. The analytical column used was a WondaSil C18 column ($4.6 \times 250 \text{ mm}$, $5 \mu\text{m}$), and CBZ and TBZ were eluted by a mixture of water with 0.1% formic acid and methanol (60:40, v/v) at a flow rate of $1.0 \text{ mL} \cdot \text{min}^{-1}$. The organic degradation intermediates of MG, CBZ, and TBZ were identified on a LX50 ultra-high performance liquid chromatograph coupled to a QSight 210 triple quad mass spectrometer (UHPLC-MS/MS, PerkinElmer, Waltham, MA). The analytes were separated on a Brownlee SPP-C18 column ($2.1 \times 100 \text{ mm}$, $2.7 \mu\text{m}$) at a flow rate of $0.4 \text{ mL} \cdot \text{min}^{-1}$. The gradient elution program for the separation of degradation products is listed in Table S1. The total organic carbon (TOC) level of the treated solution was measured on a TOC-V CPH analyzer (Shimadzu, Kyoto, Japan).

2.4. Development of chemical kinetic model

Based on the major elementary reactions involved, a chemical kinetic model was developed to describe the kinetics of MG degradation and Fe^{2+} consumption in Fenton and solar photo-Fenton processes. The model was constructed with two key assumptions: (i) $\cdot\text{OH}$ was the only reactive oxygen species contributing to the decomposition of organic species, while $\text{HO}_2\cdot$, $\text{O}_2^{\cdot-}$, and H_2O_2 had negligible contribution; and (ii) the organic radicals produced from the organic molecules attacked by $\cdot\text{OH}$ played an insignificant role in the reaction system (e.g., through reacting with iron species) due to the rather low concentration of MG.

The model for Fenton process contains 14 chemical species (including neutral molecules, ions, and radicals) and 18 elementary reactions (Table 1). Most rate constants have been reported in the literature, while the unknown values were experimentally determined or fitted with experimental data in this study. A total of 16 inorganic chemical reactions in Fenton system were included, while the other two were the reactions of MG and its hydroxylated degradation product, malachite green carbinol base (MGCB) [31], with $\cdot\text{OH}$. In solar photo-Fenton process, two additional reactions were added, namely H_2O_2 photolysis and Fe^{3+} photo-reduction (i.e., Fe^{2+} regeneration) (Table 1). The model was implemented using COPASI (ver. 4.22) [32]. In the fitting of the model with experimental data, the least mean square (LMS) was employed, which was minimized using the Evolutionary Programming Method built in COPASI.

3. Results and discussion

3.1. MG degradation in Fenton process and key reaction rate constants

The spectrophotometer only measures the light absorption of the reaction mixture at the pre-selected wavelength, and the signal must depend linearly on the concentration of the analyte (and only the analyte) in the solution to achieve on-line real time detection. MG was stable in aqueous solution at pH 3.0 (Fig. S3a), while the other species in the reaction system did not have significant light

Table 1

Summary of the elementary reactions in the chemical kinetic model for MG degradation in Fenton and solar photo-Fenton processes, and their rate constants.

No.	Reaction	Reported k ($M^{-1}\cdot s^{-1}$)	References	Model adopted k ($M^{-1}\cdot s^{-1}$)
(1)	$Fe^{2+} + H_2O_2 \rightarrow Fe^{3+} + OH^- + \cdot OH$	63–76		63
(2)	$Fe^{3+} + H_2O_2 \rightarrow Fe^{2+} + HO_2\cdot + H^+$	0.01–0.02		0.01
(3)	$Fe^{2+} + \cdot OH \rightarrow Fe^{3+} + OH^-$	$(3.0–4.3) \times 10^8$		4.3×10^8
(4)	$Fe^{2+} + HO_2\cdot (+ H^+) \rightarrow Fe^{3+} + H_2O_2$	1.2×10^6		1.2×10^6
(5)	$Fe^{3+} + HO_2\cdot \rightarrow Fe^{2+} + H^+ + O_2$	$(0.1–3.1) \times 10^5$		3.1×10^5
(6)	$Fe^{2+} + O_2\cdot^- (+ 2H^+) \rightarrow Fe^{3+} + H_2O_2$	1.0×10^7		1.0×10^7
(7)	$2 \cdot OH \rightarrow H_2O_2$	$(4.2–5.3) \times 10^9$	[9,14]	5.3×10^9
(8)	$2HO_2\cdot \rightarrow H_2O_2 + O_2$	8.3×10^5		8.3×10^5
(9)	$\cdot OH + HO_2\cdot \rightarrow H_2O + O_2$	6.6×10^9		6.6×10^9
(10)	$\cdot OH + O_2\cdot^- \rightarrow OH^- + O_2$	1.0×10^{10}		1.0×10^{10}
(11)	$HO_2\cdot + O_2\cdot^- (+ H^+) \rightarrow H_2O_2 + O_2$	9.7×10^7		9.7×10^7
(12)	$HO_2\cdot \rightarrow H^+ + O_2\cdot^-$	$(1.58–7.9) \times 10^5 s^{-1}$		$1.58 \times 10^5 s^{-1}$
(13)	$H^+ + O_2\cdot^- \rightarrow HO_2\cdot$	1.0×10^{10}		1.0×10^{10}
(14)	$\cdot OH + H_2O_2 \rightarrow HO_2\cdot + H_2O$	$(1.2–4.5) \times 10^7$		4.5×10^7
(15)	$HO_2\cdot + H_2O_2 \rightarrow \cdot OH + H_2O + O_2$	3.0		3.0
(16)	$O_2\cdot^- + H_2O_2 \rightarrow \cdot OH + OH^- + O_2$	0.13		0.13
(17)	$MG + \cdot OH \rightarrow MGCB$	$(8.76 \pm 0.63) \times 10^9 a$		$9.39 \times 10^9 b$
(18)	$MGCB + \cdot OH \rightarrow Products$	$10^7–10^{10}$	[42]	$1.0 \times 10^{10} b$
(19)	$H_2O_2 + h\nu \rightarrow 2 \cdot OH$	$4.13 \times 10^{-5} s^{-1}$	[19]	$1.36 \times 10^{-6} s^{-1}$
(20)	$Fe^{3+} + H_2O + h\nu \rightarrow Fe^{2+} + \cdot OH + H^+$	3.33×10^{-6}	[14]	5.00×10^{-7}
(21)	Organic species + $\cdot OH \rightarrow$ Inorganic species			$8.75 \times 10^8 b$

Notes:

^a Experimentally determined value in this study;

^b Value obtained by fitting with the experimental data.

absorption at the maximum absorbance wavelength of MG (617 nm) (Fig. S3b). Furthermore, a linear relationship existed between the aqueous concentration of MG and light absorbance (Fig. S3c). As a result, the light absorbance measured by the spectrophotometer could be translated directly to MG concentration. Besides, the absorbance of MG solution did not change obviously when mixed with Fe^{2+} , Fe^{3+} , or H_2O_2 (Fig. S4). These results indicate that MG did not complex with Fe^{2+} or Fe^{3+} , and it could not be oxidized by H_2O_2 alone effectively. Furthermore, the primary degradation product of MG in Fenton and solar photo-Fenton processes, MGCB, had negligible light absorbance at 617 nm (Fig. S3b). Based on the above results, the changes in absorbance at 617 nm of the reaction mixture in Fenton and solar photo-Fenton processes corresponded directly to those of MG concentration.

Although pollutant degradation in Fenton process is often observed to follow pseudo first-order kinetics, this is only true under certain conditions. Fig. S5 shows that MG degradation in Fenton process exhibited pseudo first-order kinetics when the concentration of Fenton's reagent was rather low. In contrast, MG degradation occurred in two distinct stages at much higher concentrations of Fenton's reagent. Understanding the fast kinetics in the first degradation stage is important because the treatment time can be drastically shortened (at the expense of greater Fenton's reagent consumption though).

MG degradation in Fenton process in the presence of TBA, which was added as a scavenger for $\cdot OH$ ($k_{TBA,\cdot OH} = 6.0 \times 10^8 M^{-1}\cdot s^{-1}$) [33], was carried out to validate a key assumption for the model: $\cdot OH$ is the only species responsible for the degradation of organic species. Fig. 1 shows that MG degradation was strongly inhibited by the presence of TBA (20 mM). The extent of the inhibition was close to that predicted by the model developed (discussed later), which supports that MG degradation in Fenton process results from the attack of $\cdot OH$ alone.

To refine the values of reported reaction rate constants, Fe^{2+} consumption in Fenton process in the absence of MG was measured at 0, 15, 60, 120, 180, 240, 300 s. The reaction rate constants were then systematically adjusted to best fit the model predictions with the experimentally observed Fe^{2+} concentrations under various conditions (Fig. 2a). Consequently, the rate constant values that gave the overall best performance were used in the model (Table 1).

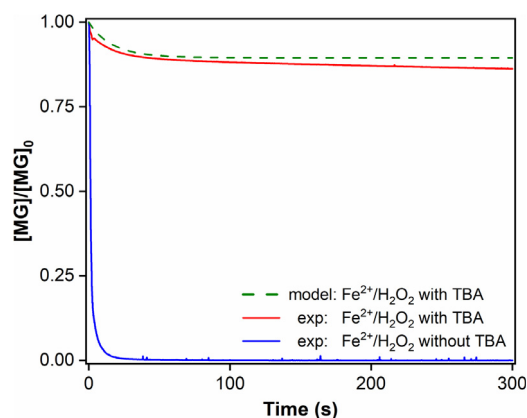


Fig. 1. Degradation of MG (6.85 μM) in Fenton process ($pH_{initial}=3.0$, $[Fe^{2+}]_0=144.0 \mu M$, and $[H_2O_2]_0=0.98$ mM) with and without the presence of TBA (20 mM), along with the model prediction for the case with the presence of TBA.

The bimolecular rate constant of the reaction between $\cdot OH$ and MG ($k_{MG,\cdot OH}$) at pH 3.0 was experimentally determined using the competition kinetic method [34]. AP, which has a well-established reaction rate constant with $\cdot OH$ ($k_{AP,\cdot OH}=5.9 \times 10^9 M^{-1}\cdot s^{-1}$) [33], was employed as the reference compound. H_2O_2 solution was irradiated by the CEL-HXF300 solar simulator (1000 $mW\cdot cm^{-2}$) to produce $\cdot OH$ (Fig. S2b). MG degradation in solar/ H_2O_2 process resulted from direct photolysis and indirect photolysis through reacting with $\cdot OH$:

$$\begin{aligned} -\frac{d[MG]}{dt} &= k_{app,MG}[MG] = k_{d,MG}[MG] + k_{i,MG}[MG] \\ &= k_{d,MG}[MG] + k_{MG,\cdot OH}[MG][\cdot OH] \end{aligned} \quad (1)$$

Similarly, the degradation kinetics of AP in solar/ H_2O_2 process could be expressed as:

$$\begin{aligned} -\frac{d[AP]}{dt} &= k_{app,AP}[AP] = k_{d,AP}[AP] + k_{i,AP}[AP] \\ &= k_{d,AP}[AP] + k_{AP,\cdot OH}[AP][\cdot OH] \end{aligned} \quad (2)$$

where $k_{app,MG}$ and $k_{app,AP}$ are the apparent rate constants of pseudo first-order degradation of MG and AP (s^{-1}) in solar/ H_2O_2 process, k_d ,

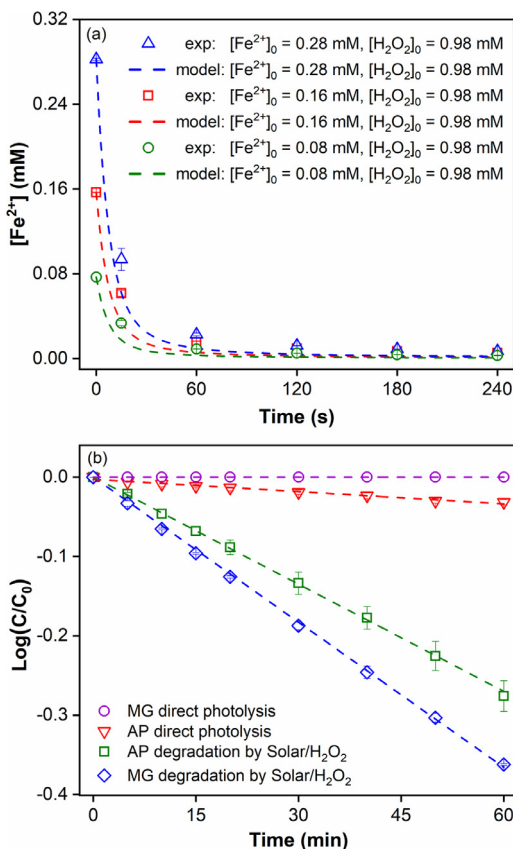


Fig. 2. Experimental determination of the key reaction rate constants in Fenton process: (a) Evolution of Fe^{2+} concentration in Fenton process at pH 3.0 in the absence of MG at different dosages of Fenton's reagent; and (b) Degradation of MG and AP in direct photolysis and solar/ H_2O_2 process (pH_{initial}=3.0, $[\text{H}_2\text{O}_2]_0=20$ mM, $[\text{MG}]_0=[\text{AP}]_0=5$ μM) under simulated sunlight irradiation.

k_{MG} and $k_{\text{d,AP}}$ are the rate constants of direct photolysis of MG and AP (s^{-1}), $k_{\text{i,MG}}$ and $k_{\text{i,AP}}$ are the rate constants of indirect photolysis of MG and AP (s^{-1}), and $k_{\text{MG},\cdot\text{OH}}$ and $k_{\text{AP},\cdot\text{OH}}$ are the bimolecular rate constants ($\text{M}^{-1}\cdot\text{s}^{-1}$) of the reaction between $\cdot\text{OH}$ and MG or AP, respectively. It could be inferred from Eqs (1) and (2) that:

$$k_{\text{MG},\cdot\text{OH}} = k_{\text{AP},\cdot\text{OH}} \times \frac{k_{\text{i,MG}}}{k_{\text{i,AP}}} = k_{\text{AP},\cdot\text{OH}} \times \frac{k_{\text{app,MG}} - k_{\text{d,MG}}}{k_{\text{app,AP}} - k_{\text{d,AP}}} \quad (3)$$

Based on the degradation kinetics of MG and AP in direct photolysis and solar/ H_2O_2 process (Fig. 2b), the value of $k_{\text{MG},\cdot\text{OH}}$ was determined to be $(8.76 \pm 0.63) \times 10^9 \text{ M}^{-1}\cdot\text{s}^{-1}$. Due to the lack of commercial MGCB, the rate constant of the reaction between $\cdot\text{OH}$ and MGCB was obtained by fitting the chemical kinetic model with experimental data.

3.2. Kinetic model of fast pollutant degradation in Fenton process

In this study, the initial concentrations of MG used were rather low (several μM) compared to the initial dosages of Fenton's reagent. The interactions between the organic intermediates and $\cdot\text{OH}$ or Fe^{3+} could have little impact on the degradation of MG or the consumption of Fenton's reagent, and were thus neglected. Table S2 lists the ordinary differential equations that correspond to the chemical reactions considered in the kinetic model. MG degradation in Fenton process under different initial conditions, along with the model fits, are presented on Fig. 3. Fig. 3a shows that increasing the initial concentration of Fe^{2+} significantly accelerated the degradation rate of MG, which is not surprising as Fe^{2+} acts as a catalyst in Fenton process. Fig. 3b indicates that increasing the initial concentration of H_2O_2 also

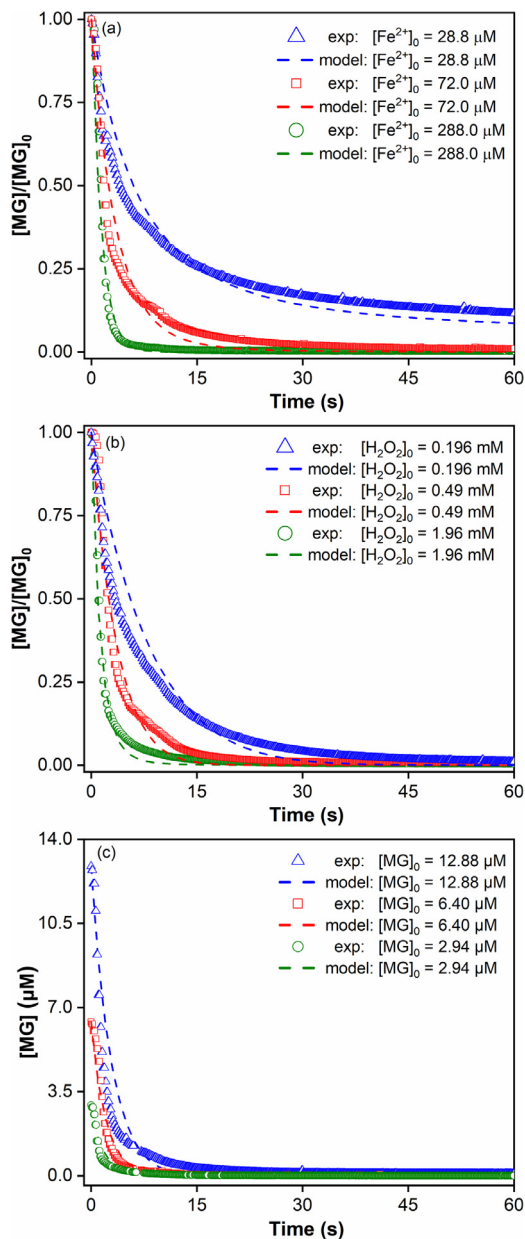


Fig. 3. MG degradation in Fenton process under different conditions, along with the model fits: (a) Impact of Fe^{2+} concentration; (b) impact of H_2O_2 concentration; and (c) impact of MG concentration. Unless noted otherwise, all experiments were conducted under the following conditions: pH_{initial}=3.0, $[\text{MG}]_0=6.85$ μM , $[\text{Fe}^{2+}]_0=144.0$ μM , and $[\text{H}_2\text{O}_2]_0=0.98$ mM.

greatly increased the degradation rate of MG. H_2O_2 is the source of $\cdot\text{OH}$ in Fenton process, thus MG degradation would be faster with more H_2O_2 . The initial concentration of MG had little impact on its degradation rate (Fig. 3c), and this can be attributed to the facts that the concentrations of MG studied were much lower than those of Fenton's reagent, thus the degradation rate of MG was almost solely determined by the concentration of $\cdot\text{OH}$ in the solution.

Overall, the chemical kinetic model established could describe the degradation kinetics of MG under all the experimental conditions evaluated, with the coefficients of determination (r^2) greater than 0.93 (Table 2). These results indicate that the model could track the evolution of major reactive species in Fenton oxidation of MG, and could well predict MG degradation under various conditions. For comparison, the empirical BMG model was also employed to fit the degradation kinetics of MG in Fenton process under different

Table 2

Summary of the coefficients of determination (r^2) of the chemical kinetic model developed in this study and the BMG model for fitting of MG degradation and Fe^{2+} consumption in Fenton and solar photo-Fenton processes.

Reaction	Experimental conditions	r^2 , chemical kinetic model	r^2 , BMG model (along with $1/m$ and $1/b$)		
MG degradation in the first stage of Fenton process	[MG] ₀ =6.85 μM , [H ₂ O ₂] ₀ =0.98 mM, Variable [Fe ²⁺] ₀	[Fe ²⁺] ₀ =28.8 μM	$r^2=0.985$	$r^2=0.997$ ($1/m=0.229$, $1/b=0.945$)	
		[Fe ²⁺] ₀ =72.0 μM	$r^2=0.967$	$r^2=0.979$ ($1/m=0.788$, $1/b=1.010$)	
	[MG] ₀ =6.85 μM , [Fe ²⁺] ₀ =144.0 μM , Variable [H ₂ O ₂] ₀	[Fe ²⁺] ₀ =288.0 μM	$r^2=0.972$	$r^2=0.868$ ($1/m=1.831$, $1/b=1.006$)	
		[H ₂ O ₂] ₀ =0.196 mM	$r^2=0.983$	$r^2=0.989$ ($1/m=0.375$, $1/b=1.027$)	
	[Fe ²⁺] ₀ =144.0 μM , [H ₂ O ₂] ₀ =0.98 mM, Variable [MG] ₀	[H ₂ O ₂] ₀ =0.49 mM	$r^2=0.974$	$r^2=0.814$ ($1/m=0.245$, $1/b=1.057$)	
		[H ₂ O ₂] ₀ =1.96 mM	$r^2=0.980$	$r^2=0.938$ ($1/m=1.557$, $1/b=1.006$)	
	MG degradation in both the first and second stages of Fenton process	[MG] ₀ =6.85 μM , Variable [Fe ²⁺] ₀ and [H ₂ O ₂] ₀	[MG] ₀ =2.94 μM	$r^2=0.951$	$r^2=0.928$ ($1/m=2.915$, $1/b=1.005$)
			[MG] ₀ =6.40 μM	$r^2=0.973$	$r^2=0.886$ ($1/m=2.118$, $1/b=1.004$)
		[MG] ₀ =12.88 μM	$r^2=0.934$	$r^2=0.949$ ($1/m=1.779$, $1/b=1.001$)	
		[Fe ²⁺] ₀ =14.4 μM , [H ₂ O ₂] ₀ =4.9 mM	$r^2=0.979$	$r^2=0.977$ ($1/m=1.600$, $1/b=0.369$)	
[Fe ²⁺] ₀ =28.8 μM , [H ₂ O ₂] ₀ =4.9 mM		$r^2=0.993$	$r^2=0.941$ ($1/m=0.635$, $1/b=0.587$)		
[Fe ²⁺] ₀ =28.8 μM , [H ₂ O ₂] ₀ =0.98 mM		$r^2=0.964$	$r^2=0.996$ ($1/m=0.158$, $1/b=0.946$)		
MG degradation in both the first and second stages of solar photo-Fenton process	[MG] ₀ =6.85 μM , Variable [Fe ²⁺] ₀ and [H ₂ O ₂] ₀	[Fe ²⁺] ₀ =14.4 μM , [H ₂ O ₂] ₀ =4.9 mM	$r^2=0.990$	$r^2=0.893$ ($1/m=0.037$, $1/b=0.465$)	
		[Fe ²⁺] ₀ =28.8 μM , [H ₂ O ₂] ₀ =4.9 mM	$r^2=0.979$	$r^2=0.925$ ($1/m=0.099$, $1/b=0.711$)	
		[Fe ²⁺] ₀ =28.8 μM , [H ₂ O ₂] ₀ =0.98 mM	$r^2=0.975$	$r^2=0.988$ ($1/m=0.133$, $1/b=0.971$)	
Consumption of Fe ²⁺ in Fenton process in the absence of organic pollutant	Variable [Fe ²⁺] ₀ and [H ₂ O ₂] ₀	[Fe ²⁺] ₀ =0.08 mM, [H ₂ O ₂] ₀ =0.98 mM	$r^2=0.964$	–	
		[Fe ²⁺] ₀ =0.16 mM, [H ₂ O ₂] ₀ =0.98 mM	$r^2=0.977$	–	
		[Fe ²⁺] ₀ =0.28 mM, [H ₂ O ₂] ₀ =0.98 mM	$r^2=0.990$	–	

conditions. The linearized form of the BMG model can be expressed as [22,35]:

$$\frac{C}{C_0} = 1 - \frac{t}{m + bt} \quad (4)$$

where C and C_0 are the concentrations of MG at time t (s) and 0, respectively, $1/m$ and $1/b$ are empirical constants that could represent the initial reaction rate and the maximum fraction of MG degradable. Fig. S6 shows that the BMG model could describe the degradation of MG under different conditions reasonably well.

3.3. Degradation of MG in solar photo-Fenton process and kinetic modeling

The absorbance of MG solution did not change obviously under simulated sunlight irradiation within the short periods of this study (Fig. S4), thus the photodegradation of MG could be neglected. The absorbance of MG solution decreased when mixed with Fe^{3+} or H_2O_2 under simulated sunlight, which is attributed to $\cdot\text{OH}$ production (Fig. S7a). The apparent degradation rate of MG in solar/ Fe^{3+} process ($3.16 \times 10^{-5} \text{ s}^{-1}$ at $[\text{Fe}^{3+}]_0=28.8 \mu\text{M}$) was much lower than that in solar/ H_2O_2 process ($1.14 \times 10^{-4} \text{ s}^{-1}$ at $[\text{H}_2\text{O}_2]_0=4.9 \text{ mM}$) (Fig. S7b), which suggests that H_2O_2 photolysis probably plays a more important role than Fe^{3+} photo-reduction in MG degradation.

Fig. 4 show that MG degradation occurred in two distinct kinetic stages under various conditions in Fenton and solar photo-Fenton processes. The slow regeneration of Fe^{2+} was the rate-limiting step that controlled the overall kinetics of MG degradation in the second stage, as indicated by the changes in Fe^{2+} concentration over time in the absence of MG (Fig. 2a). MG degradation in the second stage proceeded much slower than in the first one, thus rather long reaction time was required to achieve full decomposition. While MG degradation was negligible in the second stage of Fenton process as most of the Fe^{2+} added was already converted to Fe^{3+} , simulated sunlight irradiation greatly accelerated the oxidation kinetics. The enhancement effect of sunlight irradiation in Fenton process could be attributed to H_2O_2 photolysis, as well as Fe^{3+} photo-reduction, both of which contribute to $\cdot\text{OH}$ production (Table 1). The rate constants of H_2O_2 photolysis and Fe^{3+} photo-reduction in solar photo-Fenton process were calculated from the experimentally measured MG degradation rates in solar/ H_2O_2 process and solar/ Fe^{3+} process, and the steady-state concentrations of $\cdot\text{OH}$ in the two processes (Supplementary data).

Due to the strong light absorption of MG, the light shielding effect of MG was accounted for in the calculations of these rate constants (Supplementary data) [36].

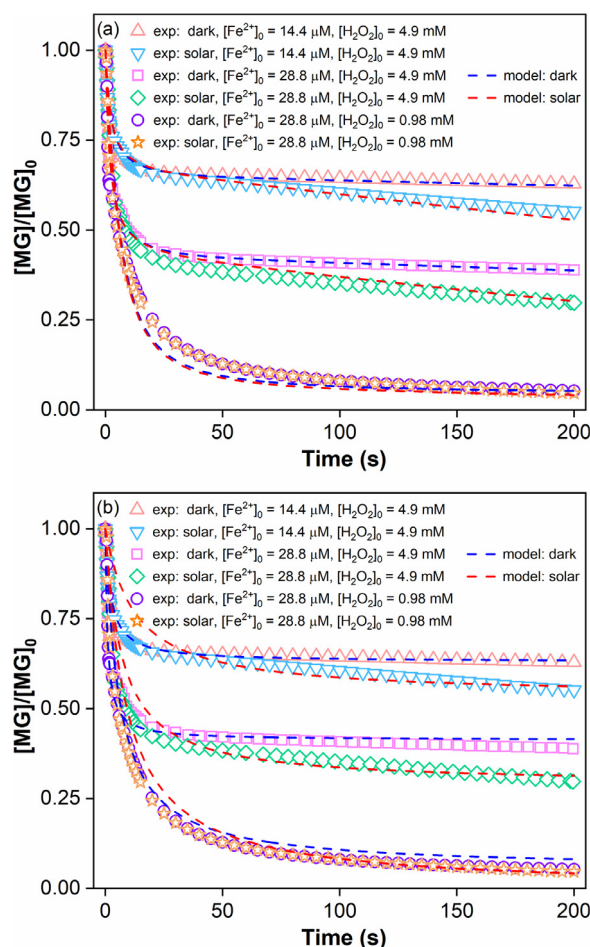


Fig. 4. Degradation of MG in Fenton and solar photo-Fenton processes, along with the model fits: (a) Chemical kinetic model developed in this study; and (b) the BMG model. Experimental conditions: $\text{pH}_{\text{initial}}=3.0$, $[\text{MG}]_0=6.85 \mu\text{M}$.

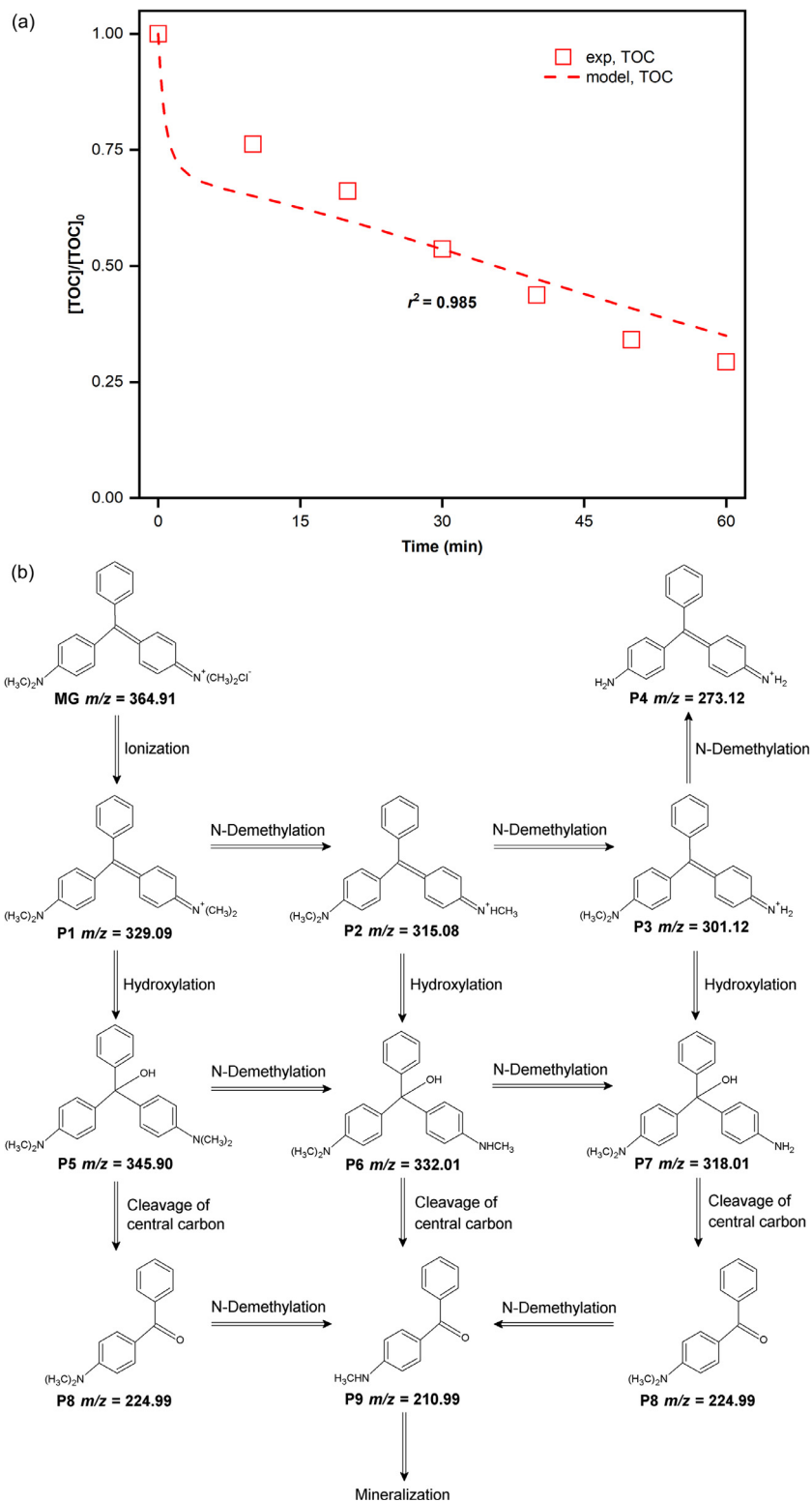


Fig. 5. Mineralization of MG in solar photo-Fenton process and its degradation pathway: (a) Solution TOC evolution during MG degradation, along with the fits of the chemical kinetic model; and (b) proposed degradation pathway of MG based on the major organic intermediates identified. Experimental condition: $\text{pH}_{\text{initial}} = 3.0$, $[\text{MG}]_0 = 6.85 \mu\text{M}$, $[\text{Fe}^{2+}]_0 = 28.8 \mu\text{M}$, and $[\text{H}_2\text{O}_2]_0 = 0.49 \text{ mM}$. A CEL-S500E7 solar simulator was used as the light source, and the irradiance was $96.8 \text{ mW}\cdot\text{cm}^{-2}$.

As shown on Fig. 4a, the chemical kinetic model could also describe the degradation kinetics of MG in solar photo-Fenton process after incorporation of the reactions of H_2O_2 photolysis and Fe^{3+} photo-reduction. Thus, it could be used to predict pollutant degradation and optimize the treatment conditions of solar photo-Fenton

process as well. The BMG model was also applied to fit the two-stage degradation kinetics of MG in Fenton and solar photo-Fenton processes. As shown on Fig. 4b, the BMG model worked well at predicting the two-stage degradation kinetics of MG in Fenton process, but the performance was poorer for that in solar photo-Fenton

Although the BMG model performed well in describing the degradation kinetics of MG in both Fenton and solar photo-Fenton processes (Table 2), it does not account for any chemical reactions involved. Such empirical models can be used as a good starting point for designing treatment conditions in practical applications. However, laboratory and pilot tests need to be conducted under a range of conditions to establish the model, and the model parameters are probably site specific. In contrast, the chemical kinetic model developed in this study accounts for all the key chemical reactions occurring in Fenton and solar photo-Fenton processes. Thus, it can adequately reflect the impact of various factors on pollutant degradation. The degradation kinetics of different organic pollutants can be predicted based on determination of the rate constant between $\cdot\text{OH}$ and the target pollutant, as demonstrated with the examples of CBZ and TBZ later. Thus, the chemical kinetic model developed in this study can be a powerful tool for predicting the kinetics of organic pollutant degradation in Fenton and solar photo-Fenton processes, as well as the optimum treatment conditions for pollutant degradation.

The mineralization of MG in solar photo-Fenton process was tracked with TOC measurements, and its kinetics was modeled by adding a simplified rate equation to the chemical kinetic model (#21 in Table 1). The TOC level of MG solution decreased continuously during the course of solar photo-Fenton process (Fig. 5a), indicating that it could be gradually mineralized in the treatment. MG mineralization could be modeled by the chemical kinetic model reasonably well, while the deviation probably resulted from the fact that the highly simplified reaction added could not adequately represent the complicated degradation steps involved in the gradual breakdown of MG molecules to inorganic species. Fig. 5b depicts the proposed degradation pathway of MG in solar photo-Fenton process based on the major organic intermediates identified (Fig. S8). Under the attack of $\cdot\text{OH}$, MG underwent a series of reactions, including hydroxylation of the central carbon, demethylation, and cleavage of the central carbon, which are similar to those observed for its oxidation in AOPs [37–39].

3.4. Model sensitivity analysis and insights on solar photo-Fenton process

Table 2 shows that the chemical kinetic model could well describe the kinetics of MG degradation and Fe^{2+} consumption in Fenton and solar photo-Fenton processes under various conditions, which demonstrates that it adequately accounts for the key reactions involved in MG degradation. Parametric sensitivity analysis was carried out to determine the sensitivity of the model with respect to the reaction parameters, and identify the key reactions in Fenton and solar photo-Fenton processes. It was performed by varying the rate constant value of a single reaction while keeping those of the others constant, and the generic sensitivity was calculated using the finite difference method.

Fig. 6 shows the results of sensitivity analysis for the model of MG degradation in Fenton and solar photo-Fenton processes. The experimental conditions evaluated were: $\text{pH}_{\text{initial}}=3.0$, $[\text{MG}]_0=6.85 \mu\text{M}$, $[\text{Fe}^{2+}]_0=14.4 \mu\text{M}$, and $[\text{H}_2\text{O}_2]_0=4.9 \text{ mM}$. Two reaction time scales were chosen for the sensitivity analysis: 30 s, which represents MG degradation in the first stage, and 200 s, which covers the degradation in both stages. Positive values of the normalized sensitivity coefficients indicate that increases in the rate constants of corresponding reactions would lower the efficiency of MG degradation, and vice versa. For Fenton oxidation of MG, the most important reaction is the attack of $\cdot\text{OH}$ ($\text{MG}+\cdot\text{OH}\rightarrow\text{MGCB}$, $k_{17}=9.39 \times 10^9 \text{ M}^{-1}\cdot\text{s}^{-1}$), and MG degradation would increase significantly with increases in the rate constant. The scavenging of $\cdot\text{OH}$ by H_2O_2 ($\cdot\text{OH}+\text{H}_2\text{O}_2\rightarrow\text{HO}_2+\text{H}_2\text{O}$, $k_{14}=4.5 \times 10^7 \text{ M}^{-1}\cdot\text{s}^{-1}$) also has significant impact on MG degradation, while increases in the rate constant would greatly reduce MG oxidation. As expected, the reactions involved in Fe^{2+} regeneration from Fe^{3+} ($\text{Fe}^{3+}+\text{H}_2\text{O}_2\rightarrow\text{Fe}^{2+}+\text{HO}_2+\text{H}^+$, $k_2=0.01 \text{ M}^{-1}\cdot\text{s}^{-1}$; $\text{Fe}^{3+}+\text{HO}_2\rightarrow\text{Fe}^{2+}+\text{H}^+\cdot\text{O}_2$,

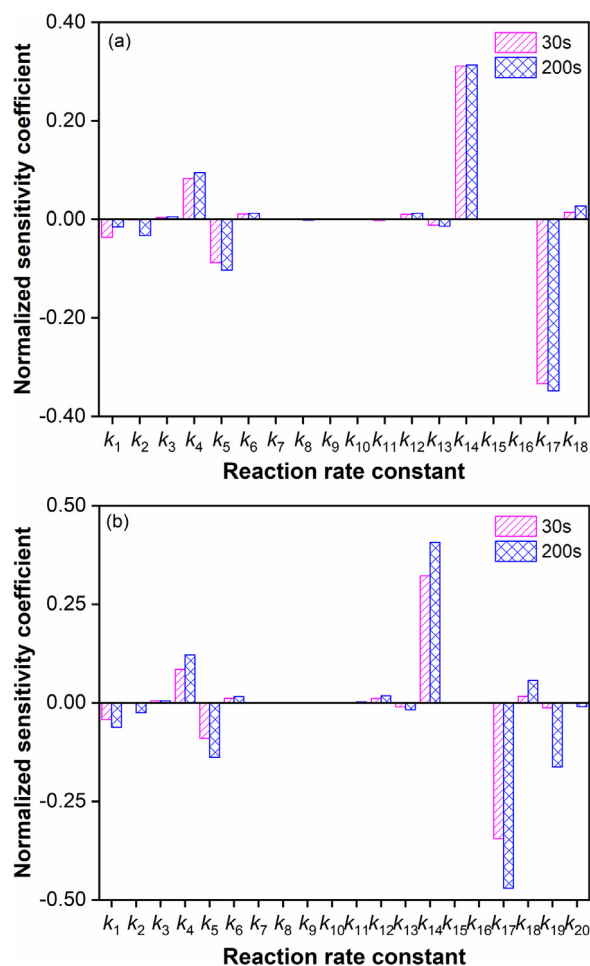


Fig. 6. The normalized sensitivity coefficients of the reaction rate constants in the chemical kinetic model at 30 and 200 s: (a) Fenton process; and (b) solar photo-Fenton process.

$k_5=3.1 \times 10^5 \text{ M}^{-1}\cdot\text{s}^{-1}$) become more important in the second stage of MG degradation compared to the first one. This can be attributed to the depletion of Fe^{2+} in the first stage and the presence of Fe^{3+} in large excess in the latter one. The values of normalized sensitivity coefficients of the other reactions are much less or even negligible, which are indicative of little contribution.

Similar to Fenton process, the two most important reactions in solar photo-Fenton process are the attack of MG by $\cdot\text{OH}$ and the scavenging of $\cdot\text{OH}$ by H_2O_2 . The reactions involved in Fe^{2+} regeneration from Fe^{3+} are also more important in the time scale of 200 s compared to 30 s (Fig. 6b). Besides, H_2O_2 photolysis ($\text{H}_2\text{O}_2+h\nu\rightarrow 2\cdot\text{OH}$, $k_{19}=8.10 \times 10^{-7} \text{ s}^{-1}$) plays a much more significant role in the overall MG degradation in the time scale of 200 s, which indicates that H_2O_2 photolysis is a key source of $\cdot\text{OH}$ in the second stage of solar photo-Fenton process. In contrast, the values of normalized sensitivity coefficient for Fe^{3+} photo-reduction ($\text{Fe}^{3+}+\text{H}_2\text{O}+h\nu\rightarrow\text{Fe}^{2+}+\text{OH}+\text{H}^+$, $k_{20}=3.21 \times 10^{-7} \text{ M}^{-1}\cdot\text{s}^{-1}$) are very low in both two time scales, suggesting that Fe^{3+} photo-reduction contributes little to MG oxidation. These results reveal that Fe^{3+} photo-reduction plays a minor role compared to H_2O_2 photolysis in the enhancement of MG degradation in solar photo-Fenton process. This can be attributed to the much lower concentration of Fe^{3+} compared to H_2O_2 , as well as the lower photo-reactivity of ferric species compared to H_2O_2 . For example, the quantum yield of FeOH^{2+} under UV irradiation is $(0.21\pm 0.04) \text{ mol}\cdot\text{Einstein}^{-1}$ [40], while that of H_2O_2 is $0.50 \text{ mol}\cdot\text{Einstein}^{-1}$ [41]. Together, with the help of the chemical kinetic model, the contribution from Fe^{3+} photo-reduction and H_2O_2 photolysis, both of which

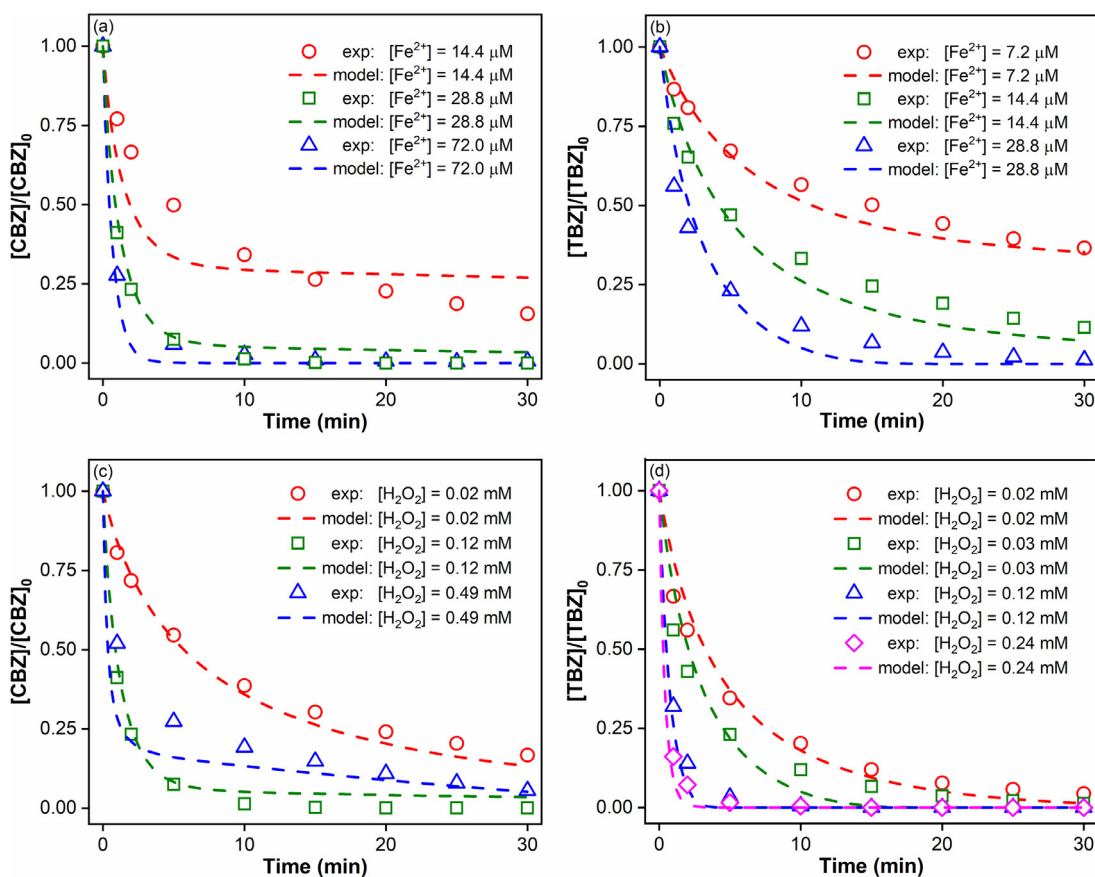


Fig. 7. Degradation of CBZ and TBZ in solar photo-Fenton process under different conditions, along with the model fits: (a) Impact of Fe^{2+} concentration on CBZ degradation; (b) impact of Fe^{2+} concentration on TBZ degradation; (c) impact of H_2O_2 concentration on CBZ degradation; and (d) impact of H_2O_2 concentration on TBZ degradation. Unless noted otherwise, all experiments were conducted under the following conditions: $\text{pH}_{\text{initial}}=3.0$, $[\text{CBZ}]_0=[\text{TBZ}]_0=6.85 \mu\text{M}$, $[\text{Fe}^{2+}]_0=28.8 \mu\text{M}$, with $[\text{H}_2\text{O}_2]_0=0.12 \text{ mM}$ in CBZ degradation and $[\text{H}_2\text{O}_2]_0=0.03 \text{ mM}$ in TBZ degradation.

produce $\cdot\text{OH}$, to pollutant degradation in solar photo-Fenton process was quantitatively evaluated for the first time.

3.5. Validation of the chemical kinetic model with CBZ and TBZ degradation

To further evaluate the performance of the chemical kinetic model, degradation of CBZ and TBZ in solar photo-Fenton process was studied. Fig. 7 depicts the impact of Fe^{2+} and H_2O_2 concentrations on CBZ and TBZ degradation in solar photo-Fenton process. Under suitable conditions, both compounds could be fully degraded within 30 min. The rate constants of the reactions between $\cdot\text{OH}$ and CBZ or TBZ determined with the competition kinetic method were 3.34×10^9 and $9.56 \times 10^9 \text{ M}^{-1}\cdot\text{s}^{-1}$, respectively (Fig. S9), which are in the same bulk range of the rate constants observed (10^7 to $10^{10} \text{ M}^{-1}\cdot\text{s}^{-1}$) between $\cdot\text{OH}$ and organic compounds [42]. Similar to that for MG, chemical kinetic models for CBZ and TBZ degradation in solar photo-Fenton process could be established (Tables S3 and S4). Fig. 7 also shows that CBZ and TBZ degradation in solar photo-Fenton process could be well predicted by the chemical kinetic models using the experimentally determined rate constants.

Based on the major organic degradation intermediates identified (Figs. S11 and S12), the probable degradation pathways of CBZ and TBZ in solar photo-Fenton process can be delineated (Fig. S13). The main degradation pathway of CBZ includes hydroxylation, carboxylation, and cleavage of the C-N bond of the amide group, while that of TBZ involves hydroxylation of the benzene ring, the cleavage of C=C, C=N, and C-N, and methylation. As shown in Fig. 8, partial mineralization of CBZ and TBZ occurred in solar photo-Fenton process. Based

on fitted rate constants of 6.14×10^8 and $5.81 \times 10^8 \text{ M}^{-1}\cdot\text{s}^{-1}$ for the reactions between $\cdot\text{OH}$ and the degradation products of CBZ or TBZ, respectively, the mineralization kinetics of these compounds could also be described by the chemical kinetic model.

4. Conclusions

This study investigated the fast kinetics of pollutant degradation in Fenton and solar photo-Fenton processes using MG as a model compound and continuous on-line spectrophotometric detection. Such combination allows monitoring of the rapid changes in pollutant concentration that could not be tracked with conventional time-sampling techniques. With Fenton's reagent in large excess, MG degradation occurred in a rapid first stage and a rather slow second stage, while sunlight irradiation significantly enhanced MG degradation in the second stage. The chemical kinetic model established in this study could well describe the kinetics of MG degradation in Fenton and solar photo-Fenton processes under widely varying conditions, and could be adapted to model its mineralization kinetics. Results of sensitivity analysis revealed that sunlight irradiation enhanced MG degradation in Fenton process primarily through the additional $\cdot\text{OH}$ produced from H_2O_2 photolysis, while the regeneration of Fe^{2+} through Fe^{3+} photo-reduction had little contribution. The chemical kinetic model could also predict the degradation and mineralization kinetics of two benzimidazoles (CBZ and TBZ) in solar photo-Fenton process. The improved understanding on the fast kinetics of pollutant degradation and the chemical kinetic model could help optimize the treatment conditions for MG and other

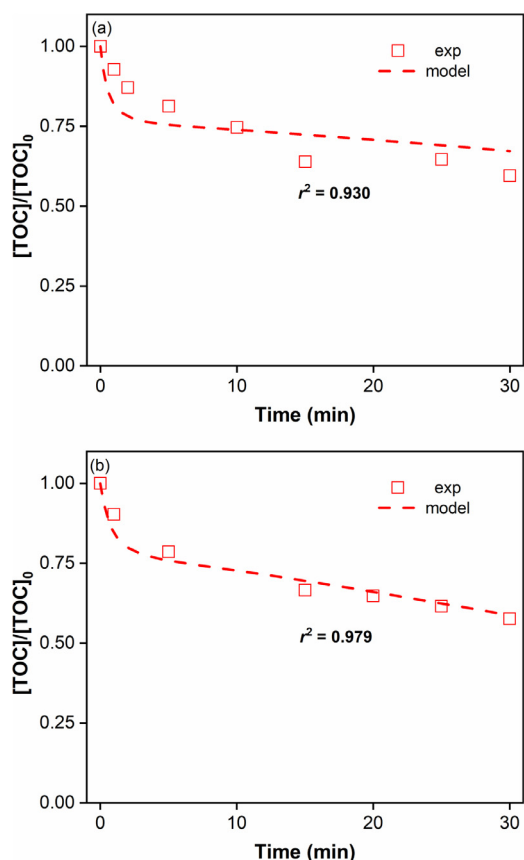


Fig. 8. Experimental data and model fits of solution TOC evolution during CBZ and TBZ degradation in solar photo-Fenton process. Experimental condition: $\text{pH}_{\text{initial}}=3.0$, $[\text{CBZ}]_0=[\text{TBZ}]_0=6.85 \mu\text{M}$, $[\text{Fe}^{2+}]_0=28.8 \mu\text{M}$, and $[\text{H}_2\text{O}_2]_0=0.49 \text{ mM}$. A CEL-S500E7 solar simulator was used as the light source, and the total irradiance was $96.8 \text{ mW}\cdot\text{cm}^{-2}$.

refractory organic compounds in Fenton and solar photo-Fenton processes.

Declaration of Competing Interest

The authors declare that they have no known competing financial interests or personal relationships that could have appeared to influence the work reported in this paper.

Acknowledgments

The constructive comments of anonymous reviewers on an earlier version of this manuscript are greatly appreciated. This study was supported in parts by the Natural Science Foundation of China (Grant Nos. U2006212 and 41725015).

Supplementary materials

Supplementary material associated with this article can be found in the online version at doi:[10.1016/j.jtice.2021.05.011](https://doi.org/10.1016/j.jtice.2021.05.011).

References

- [1] Hu Y, He Y, Cheng H. Microwave-induced degradation of *N*-nitrosodimethylamine (NDMA) sorbed in zeolites: Effect of mineral surface chemistry and non-thermal effect of microwave. *J Clean Prod* 2018;174:1224–33.
- [2] Sun B, Hu Y, Cheng H. Microwave-induced degradation as a novel treatment for destruction of decabromodiphenyl ether sorbed on porous minerals. *Chem Eng J* 2020;391:123550.
- [3] Xie X, Zhao W, Hu Y, Xu X, Cheng H. Permanganate oxidation and ferric ion precipitation ($\text{KMnO}_4\text{-Fe(III)}$) process for treating phenylarsenic compounds. *Chem Eng J* 2019;357:600–10.
- [4] Xie X, Hu Y, Cheng H. Rapid degradation of *p*-arsanilic acid with simultaneous arsenic removal from aqueous solution using Fenton process. *Water Res* 2016;89:59–67.
- [5] Nogueira RFP, Silva MRA, Trovó AG. Influence of the iron source on the solar photo-Fenton degradation of different classes of organic compounds. *Sol Energy* 2005;79:384–92.
- [6] Burbano AA, Dionysiou DD, Suidan MT, Richardson TL. Oxidation kinetics and effect of pH on the degradation of MTBE with Fenton reagent. *Water Res* 2005;39:107–18.
- [7] Cui K, Yi H, Zhou Z, Zhuo Q, Bing Y, Guo Q, et al. Fenton oxidation kinetics and intermediates of nonylphenol ethoxylates. *Environ Eng Sci* 2014;31:217–24.
- [8] Wang S. A Comparative study of Fenton and Fenton-like reaction kinetics in decolorisation of wastewater. *Dyes Pigm* 2008;76:714–20.
- [9] Du Y, Zhou M, Lei L. Kinetic model of 4-CP degradation by Fenton/ O_2 system. *Water Res* 2007;41:1121–33.
- [10] Segura C, Zaror C, Mansilla HD, Mondaca MA. Imidacloprid oxidation by photo-Fenton reaction. *J Hazard Mater* 2008;150:679–86.
- [11] Paiva VAB, Paniagua CES, Ricardo IA, Goncalves BR, Martins SP, Daniel D, et al. Simultaneous degradation of pharmaceuticals by classic and modified photo-Fenton process. *J Environ Chem Eng* 2018;6:1086–92.
- [12] Gonzalez GC, Julcour C, Chaumat H, Jauregui-Haza U, Delmas H. Degradation of 2,4-dichlorophenoxyacetic acid by photolysis and photo-Fenton oxidation. *J Environ Chem Eng* 2018;6:874–82.
- [13] Romero V, Acevedo S, Marco P, Gimenez J, Esplugas S. Enhancement of Fenton and photo-Fenton processes at initial circumneutral pH for the degradation of the beta-blocker metoprolol. *Water Res* 2016;88:449–57.
- [14] Kusic H, Koprivanac N, Horvat S, Bakija S, Bozic AL. Modeling dye degradation kinetic using dark- and photo-Fenton type processes. *Chem Eng J* 2009;155:144–54.
- [15] Baba Y, Yatagai T, Harada H, Kawase Y. Hydroxyl radical generation in the photo-Fenton process: Effects of carboxylic acids on iron redox cycling. *Chem Eng J* 2015;277:229–41.
- [16] Gallard H, De Laat J. Kinetic modelling of $\text{Fe(III)/H}_2\text{O}_2$ oxidation reactions in dilute aqueous solution using atrazine as a model organic compound. *Water Res* 2000;34:3107–16.
- [17] Qiu S, He D, Ma J, Liu T, Waite TD. Kinetic modeling of the electro-Fenton process: Quantification of reactive oxygen species generation. *Electrochim Acta* 2015;176:51–8.
- [18] Duysterberg CK, Waite TD. Process optimization of Fenton oxidation using kinetic modeling. *Environ Sci Technol* 2006;40:4189–95.
- [19] Kusic H, Koprivanac N, Bozic AL, Selanec I. Photo-assisted Fenton type processes for the degradation of phenol: A kinetic study. *J Hazard Mater* 2006;136:632–44.
- [20] Chan KH, Chu W. Modeling the reaction kinetics of Fenton's process on the removal of atrazine. *Chemosphere* 2003;51:305–11.
- [21] Chu W, Kwan CY, Chan KH, Chong C. An unconventional approach to studying the reaction kinetics of the Fenton's oxidation of 2,4-dichlorophenoxyacetic acid. *Chemosphere* 2004;57:1165–71.
- [22] Behnajady MA, Modirshahla N, Ghanbary F. A kinetic model for the decolorization of C.I. Acid Yellow 23 by Fenton process. *J Hazard Mater* 2007;148:98–102.
- [23] Basturk E, Karatas M. Advanced oxidation of Reactive Blue 181 solution: A comparison between Fenton and sono-Fenton process. *Ultrason Sonochem* 2014;21:1881–5.
- [24] Khan N-U-H, Bhatti HN, Iqbal M, Nazir A. Decolorization of Basic Turquoise Blue X-GB and Basic Blue X-GRRL by the Fenton's Process and its Kinetics. *Z Phys Chem* 2019;233:361–73.
- [25] Ramos MDN, Sousa LA, Aguiar A. Effect of cysteine using Fenton processes on decolorizing different dyes: a kinetic study. *Environ Technol LA*. Sousa, A. Aguiar, Effect of cysteine using Fenton processes on decolorizing different dyes: a kinetic study. *Environ Technol* 2020. doi: 10.1080/09593330.2020.1776402.
- [26] Behrouzeh M, Abbasi M, Osfouri S, Dianat MJ. Treatment of DMSO and DMAC wastewaters of various industries by employing Fenton process: Process performance and kinetics study. *J Environ Chem Eng* 2020;8:103597.
- [27] Tunc S, Gürkan T, Duman Q. On-line spectrophotometric method for the determination of optimum operation parameters on the decolorization of Acid Red 66 and Direct Blue 71 from aqueous solution by Fenton process. *Chem Eng J* 2012;181–2:431–42.
- [28] Tunc S, Duman Q, Gürkan T. Monitoring the decolorization of Acid Orange 8 and Acid Red 44 from aqueous solution using Fenton's reagents by online spectrophotometric method: Effect of operation parameters and kinetic study. *Ind Eng Chem Res* 2013;52:1414–25.
- [29] Klassen NV, Marchington D, McGowan HCE. H_2O_2 Determination by the I_3 method and by KMnO_4 titration. *Anal Chem* 1994;66:2921–5.
- [30] Tamura H, Goto K, Yotsuyanagi T, Nagayama M. Spectrophotometric determination of iron(II) with 1,10-phenanthroline in the presence of large amounts of iron (III). *Talanta* 1974;21:314–8.
- [31] Sires I, Guivarch E, Oturan N, Oturan MA. Efficient removal of triphenylmethane dyes from aqueous medium by in situ electrogenerated Fenton's reagent at carbon-felt cathode. *Chemosphere* 2008;72:592–600.
- [32] Hoops S, Sahle S, Gauges R, Lee C, Pahle J, Simus N, et al. COPASI - a complex pathway simulator. *Bioinformatics* 2006;22:3067–74.
- [33] Buxton GV, Greenstock CL, Helman WP, Ross AB. Critical review of rate constants for reactions of hydrated electrons, hydrogen atoms and hydroxyl radicals ($\text{OH}^\bullet/\text{O}^\bullet$) in aqueous solution. *J Phys Chem Ref Data* 1988;17:513–886.
- [34] Edlund BL, Arnold WA, McNeill K. Aquatic photochemistry of nitrofurant antibiotic. *Environ Sci Technol* 2006;40:5422–7.

- [35] Zhao W, Cheng H, Tao S. Structure–reactivity relationships in the adsorption and degradation of substituted phenylarsonic acids on birnessite (δ -MnO₂). *Environ Sci Technol* 2020;54:1475–83.
- [36] Zhang Z, Xie X, Yu Z, Cheng H. Influence of chemical speciation on photochemical transformation of three fluoroquinolones (FQs) in water: Kinetics, mechanism, and toxicity of photolysis products. *Water Res* 2019;148:19–29.
- [37] He W, Sun Y, Jiang G, Li Y, Zhang X, Zhang Y, et al. Defective Bi₄MoO₉/Bi metal core/shell heterostructure: Enhanced visible light photocatalysis and reaction mechanism. *Appl Catal B-Environ* 2018;239:619–27.
- [38] Liu J, Wang G, Li B, Ma X, Hu Y, Cheng H. A high-efficiency mediator-free Z-scheme Bi₂MoO₆/AgI heterojunction with enhanced photocatalytic performance. *Sci Total Environ* 2021;784:147227.
- [39] Wang G, Ma X, Liu J, Qin L, Li B, Hu Y, et al. Design and performance of a novel direct Z-scheme NiGa₂O₄/CeO₂ nanocomposite with enhanced sonocatalytic activity. *Sci Total Environ* 2021;741:140192.
- [40] Nadochenko VA, Kiwi J. Photolysis of FeOH²⁺ and FeCl²⁺ in aqueous solution. Photodissociation kinetics and quantum yields. *Inorg Chem* 1998;37:5233–8.
- [41] Kusic H, Peternel I, Ukic S, Koprivanac N, Bolanca T, Papic S, et al. Modeling of iron activated persulfate oxidation treating reactive azo dye in water matrix. *Chem Eng J* 2011;172:109–21.
- [42] TNG Borhani, Saniedanesh M, Bagheri M, Lim JS. QSPR prediction of the hydroxyl radical rate constant of water contaminants. *Water Res* 2016;98:344–53.